FAST AND ACCURATE SEGMENTATION OF THE LV IN MR VOLUMES USING A DEFORMABLE MODEL WITH DYNAMIC PROGRAMMING

Carlos Santiago, Jacinto C. Nascimento, Jorge S. Marques

Institute for Systems and Robotics (ISR/IST), LARSyS, Instituto Superior Técnico,
Universidade Lisboa, Portugal

ABSTRACT

This paper proposes a new approach for the segmentation of the endocardium of the left ventricle using short axis magnetic resonance (MR) images. The proposed method contains two main stages. First, each image is converted to polar coordinates, and an edge map is computed from the transformed image. Then, the contour of the left ventricle (LV) is estimated by computing the optimal path along the edge map, using a dynamic programming approach. The system is evaluated on a public database comprising 660 magnetic resonance volumes and the results testify its usefulness both in terms of running time and accuracy. The proposed methodology is able to segment a whole volume in 1.5 seconds achieving an average Dice similarity coefficient of 85.9% (8.3%), which compares favorably with related state-of-the-art methods.

Index Terms— Segmentation, cardiac MRI, dynamic programming

1. INTRODUCTION

This paper proposes a new methodology tailored to provide a fast and accurate segmentation of the left ventricle (LV) in MR volumes. The goal is to help speed up the manual segmentation of the LV, which is a laborious and time consuming task required in most clinical practices.

The problem is addressed by sequentially analyzing the slices (*i.e.*, 2D images) of a volume. First, an initial guess of the location of the LV in the basal slice is provided, by giving an estimate of the center and radius of the endocardium in that particular slice. This segmentation is then propagated to the next slice as an initial guess, and the process is repeated until the whole volume has been segmented.

Two main assumptions are taken into account in the proposed approach: (i) that the LV boundary is approximately circular in each slice of the MR volume; and (ii) that the contour is associated to the presence of edges in the image. The algorithm is characterized by two stages. The first stage aims to obtain an edge map, whose valleys correspond to the LV

boundary. The second stage uses dynamic programming (DP) [1, 2] to determine the optimal path along the edge map. This latter stage will provide the delineation of the LV contour.

2. RELATED WORK

The existing literature on the estimation of the LV in MR images is vast. Yet, this is an open problem, as testified by several surveys (*e.g.* [3, 4]). This happens because this particular problem faces many difficulties, among which: (i) the LV border is not always located at the image edges; (ii) the blood flow leads to the presence of the gray level inhomogeneities; and (iii) the presence of papillary muscles and trabeculations, or wall irregularities, inside the heart chambers, that have the same intensity profile as the endocardium. These difficulties make most image features (*e.g.*, image gradient) unable to detect the entire LV boundary. Several works have been proposed to tackle the above difficulties. For instance, [5] introduces low-level image processing techniques incorporating anatomical knowledge to provide the convex hull of the shape, or adopting morphological operations as in [6]. The approach proposed in [7] is based on a thresholding operation to discern between outer and inner regions. In this line of research, DP is also a common choice to separate the two regions. Geiger et al. [8] were one of the first to use DP and several others have since followed (see for instance [1, 9, 10]).

The proposed framework is inspired in [2], where DP is used to extract the desired boundary. We combine this approach with the advantages of the DP method proposed in [1]. This strategy significantly reduces the computational complexity, and thus, is able to obtain a fast LV segmentation without compromising the accuracy of the results.

3. PROPOSED APPROACH

The proposed methodology comprises two main stages. First, it estimates an edge map by analyzing the MR image in polar coordinates. This process is illustrated in Fig. 1. Second, the delineation of the LV contour is obtained by using DP to place the contour along the valleys of the edge map. The following sections describe these two stages in detail.
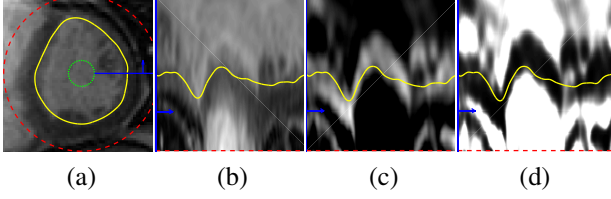
Fig. 1. Edge map estimation: (a) original MR image, $I(x, y)$; (b) image in polar coordinates, $I_{\mathcal{P}}(r, \theta)$; (c) image gradient, $I_{\mathcal{G}}(r, \theta)$; and (d) edge map, $e_{\text{MAP}}(r, \theta)$. The yellow line is the LV segmentation (computed in (d)). The green and red lines correspond to the minimum and maximum radius, respectively, and the blue line and arrow help illustrate the conversion to polar coordinates.

3.1. Edge map estimation

Since the LV boundary is roughly a circular shaped curve, the edge map is computed in polar coordinates. This means that, the intensity of a given pixel (r, θ) is obtained by computing $I_{\mathcal{P}}(r, \theta) = I(x, y)$, as

$$x = c_x + r\cos(\theta), \qquad y = c_y + r\sin(\theta). \qquad (1)$$

where (x, y) are the Cartesian coordinates, and $\mathbf{c} = [c_x, c_y]^\top \in \mathbb{R}^2$ are the coordinates of the LV center that are provided by the user.

The intensity value of $I_{\mathcal{P}}(r, \theta)$ are obtained using bilinear interpolation (see [11] for details) [1]. The domain $\mathcal{D}_r \times \mathcal{D}_\theta$ in which the polar coordinates, (r, θ), are defined in the image $I_{\mathcal{P}}(r, \theta)$ are given as

$$\mathcal{D}_r = \{r_1, \ldots, r_M \in \mathbb{R} : r_i = r_{\min} + (i-1)\Delta r\}$$
$$\mathcal{D}_\theta = \{\theta_1, \ldots, \theta_N \in [0, 2\pi] : \theta_j = (j-1)\Delta\theta\}, \qquad (2)$$

where $\Delta r = \frac{r_{\max} - r_{\min}}{M-1}$, and $\Delta\theta = \frac{2\pi}{N-1}$; $r_{\max}$ and $r_{\min}$ define the width of the ring within which the LV border is expected to be found. Note that the first and last column of $I_{\mathcal{P}}$ correspond to the same positions, *i.e.*, $\theta_1 = \theta_N = 2\pi$.

After the polar image $I_{\mathcal{P}}(r, \theta)$ has been computed, a high pass filter is applied to obtain a gradient image $I_{\mathcal{G}}(r, \theta)$, shown in Fig. 1 (c). In the gradient image, high intensity pixels are correlated with the presence of an edge along that particular radial line. Finally, to obtain a normalized edge map from $I_{\mathcal{G}}(r, \theta)$, the following sigmoid function is used:

$$e_{\text{MAP}}(r, \theta) = (1 + \exp(\lambda(I_{\mathcal{G}}(r, \theta) - k)))^{-1}, \qquad (3)$$

where $k > 0$ and $\lambda > 0$ control the inflection point and the sharpness of the sigmoid, respectively. In this work, the values for these parameters were empirically determined and set to $k = 20$ and $\lambda = 0.04$. The above normalized edge map $e_{\text{MAP}}(r, \theta) \in [0, 1]$ assigns a small cost to edges (supposedly where the LV border is located) and a high cost to the remaining regions of the image $I_{\mathcal{G}}(r, \theta)$.

---

[1] This interpolation is necessary since the transformation does not guarantee that (x, y) take integer values in the image.

3.2. Contour estimation

The delineation of the LV contour is obtained in the second stage of the algorithm. This is achieved by fitting a curve to the edge map, e_{MAP}, that stretches from the left border to right, and that tries to follow the valleys of the image (see Fig. 1 (d)).

If we define a parametric curve, say $\widehat{\mathbf{x}}(s)$, (where $0 \leq s \leq 1$ is the curve parameter), the goal is to find the curve such that

$$\widehat{\mathbf{x}} = \arg\min_{\mathbf{x}} \mathcal{E}(\mathbf{x}), \qquad (4)$$

where $\mathcal{E}$ is an energy function defined as

$$\mathcal{E}(\mathbf{x}) = \int_s E_{\text{int}}(\mathbf{x}(s)) + E_{\text{ext}}(\mathbf{x}(s))\, ds. \qquad (5)$$

E_{int} is the internal energy, that imposes smoothness on the curve estimates $\widehat{\mathbf{x}}(s)$, and E_{ext} is the external energy, which is obtained from the image. This formalism in known as deformable or active contour model (*e.g.*, [12, 13]). In this paper, we address this problem by using DP. The edge map e_{MAP} can be viewed as a $M \times N$ matrix, and the goal is to find a curve $\widehat{\mathbf{r}} = [r(1), ..., r(N)]^\top$ (a sequence of radius values), such that $r(j) \in \mathcal{D}_r$ corresponds to the LV radius for angle θ_j. The problem formulation is similar to (4), but now we are considering a discrete variables that are defined in polar coordinates (r, θ),

$$\mathcal{E}(\mathbf{r}) = \sum_{j=1}^{N} E_{\text{int}}(r(j)) + E_{\text{ext}}(r(j)). \qquad (6)$$

The data term is now given by

$$E_{\text{ext}}(r(j)) = e_{\text{MAP}}(r(j), \theta_j), \qquad (7)$$

and the internal energy term is given as

$$E_{\text{int}}(r(j)) = d(r(j-1), r(j))$$
$$= \begin{cases} 0 & \text{if} \quad |r(j) - r(j-1)| = 0 \\ \eta & \text{if} \quad |r(j) - r(j-1)| = \Delta r \quad (8) \\ \infty & \text{otherwise.} \end{cases}$$

The former corresponds to the edge map, whose minima are located along its valleys, and the latter constrains the curve, $\mathbf{r}$, by penalizing large differences between consecutive pairs $(r(j-1), r(j))$, with $E_{\text{int}}(r(1)) = 0$.

Putting (7), (8) together, (6) can be rewritten as

$$\mathcal{E}(\mathbf{r}) = e_{\text{MAP}}(r(1), \theta_1) +$$
$$+ \sum_{j=2}^{N} e_{\text{MAP}}(r(j), \theta_j) + d(r(j-1), r(j)). \qquad (9)$$

Finally, the optimal contour is computed as

$$\begin{aligned} \widehat{\mathbf{r}} = \quad &\arg\min_{\mathbf{r}} \quad \mathcal{E}(\mathbf{r}) \\ &\text{s.t.} \quad r(1) = r(N) \qquad (10) \\ &\qquad r(j) \in \mathcal{D}_r, \ j = 1, \ldots, N \end{aligned}$$

where $\mathcal{D}_r$ is defined in (2).

To solve (10), we rewrite (9) as follows

$$\mathcal{E}_j(r_i) = e_{\mathrm{MAP}}(r_i, \theta_j) + \min_{\rho \in \mathcal{D}_r} \left[d(\rho, r_i) + \mathcal{E}_{j-1}(\rho) \right], \quad (11)$$

which can be viewed as the optimal cost to reach the position (r_i, θ_j) in e_{MAP}. The cost $\mathcal{E}_j(r_i)$ can thus be recursively obtained by computing the optimal costs of reaching the previous column, $\mathcal{E}_{j-1}(r_i)$, $i = 1, \dots, M$. To guarantee that the solution starts and ends at a specific position $r(1)$, we simply set $e_{\mathrm{MAP}}(r_i, \theta_1) = \infty, \forall_{r_i \in \mathcal{D}_r} : r_i \neq r(1)$. The final procedure, denoted as *Forward-Backward* algorithm (FB-A), is the following [1, 2]:

1. *Forward step*: Compute the optimal costs of all the curves that start at θ_1 and end at θ_N, using (11), and, for each local minimization problem (second term in (11)), store the corresponding radii

$$\phi(r_i, \theta_j) = \arg \min_{\rho \in \mathcal{D}_r} d(\rho, r_i) + \mathcal{E}_{j-1}(\rho). \qquad (12)$$

2. *Backward step*: Trace back the optimal path that ends at $r(N) = r(1)$, using the stored radii

$$r(N) = r(1) \qquad (13)$$

$$r(\tau - 1) = \phi(r(\tau), \theta_\tau), \quad \tau = N, ..., 2 \qquad (14)$$

To obtain the object contour we have to: (i) run the FB-A for all possible starting points $r(1) \in \mathcal{D}_r$, obtaining several paths, and (ii) select the path with the lowest global cost (computed using (9)). Notice, however, that the above procedure can lead to a high computational cost, since it must be applied for all starting positions, which increases with M. Alternatively, [1] proposes to mitigate this limitation by running the FB-A algorithm only twice (2-Loop algorithm). Basically, this algorithm assumes that the optimal path close to the column $j = N/2$ does not depend on the choice of the starting point $r(1)$, since $r(1)$ is far from $r(N/2)$. This means that the optimal value obtained for $r(N/2)$ will be the same whatever the choice of the starting point $r(1)$ is. Hence, the algorithm FB-A needs to be run only a second time starting at the optimal solution $r(N/2)$. The procedure is summarized as follows:

(i) it runs the FB-A with some initial point $r(1)$; then

(ii) it switches the two halves of the edge map, and runs FB-A starting at the solution obtained in (i) at the location $r'(1) = r(N/2)$; and finally

(iii) the two halves of the new optimal path, obtained in (ii), are switched back to the original order.

The 2-Loop procedure is illustrated in Fig. 2. It is possible to see in Fig. 2 (a) that even if we choose $r(1) = 1$, which
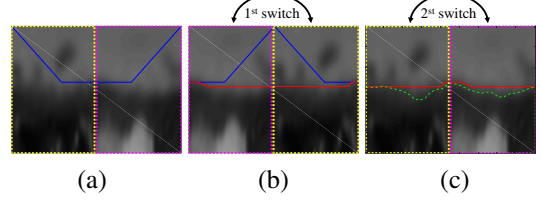

(a)   (b)   (c)

Fig. 2. 2-Loop algorithm. The blue line depicts the solution of A1 with initial position $r(1) = r_{\min}$; the red line depicts the solution of A1 on the reordered edge map with initial position $r'(1) = r(N/2)$; the green dashed line represents the ground truth segmentation. The yellow and magenta rectangles and black arrows illustrate the switching of the two halves of the edge map and the optimal path.

is very far from the LV border, in the first run, the optimal path near the column $j = N/2$ matches the desired solution (shown in green in (c)). This indicates that the assumption on which the 2-Loop algorithm is based is valid (at least for some sufficiently large N).

4. EXPERIMENTAL SETUP

The proposed approach is evaluated on a public benchmark dataset of cardiac MR sequences [14]. This dataset comprises 33 sequences of volumes concerning both healthy and disease cases. Each sequence contains 20 volumes, covering the systole and diastole phases of the cardiac cycle. Each volume contains a number of slices varying from 5 to 10, with a spacing of 6-13 mm. Each slice is a 256×256 image, with a resolution of 0.93-1.64 mm. The ground truth (GT) of the dataset is already provided.

For evaluation purposes, a quantitative evaluation of the LV segmentation is conducted. To accomplish this two metrics are used: (i) the volumetric Dice coefficient, and (ii) the average perpendicular distance (AV). The Dice coefficient measures the percentage of the overlap between the proposed segmentation and the GT (*i.e.*, Dice = 1 is a perfect match between the estimated contours and the GT). The AV measure corresponds to the average distance between each point in the estimated contour and the closest GT point. Also, we show the results excluding the *bad segmentations* (*i.e.*, results with $d_{\mathrm{AV}} > 5$ mm), jointly with the corresponding percentage of *good segmentations*. In the Section 5 we show the performance of the algorithms labeled as FB-A and 2-Loop using the above mentioned metrics, as well as the computational performance of each method.

5. RESULTS

Table 1 shows the statistical results of the two approaches FB-A and 2-Loop. In terms of the segmentation accuracy, both approaches exhibit a similar performance. However, in terms of running time, the 2-Loop is far superior, as shown in the last column of Table 1.

Table 1. Statistical evaluation of the proposed algorithms. For each algorithm, the table shows the results for all the segmentations (dashed entries in the "% Good" column) and excluding segmentations with AV > 5 mm. Each entry shows the mean value and standard deviation.

	Dice (%)	AV (mm)	% Good	$\frac{\text{Time}}{\text{Volume}}$ (s)
FB-A	83.5 (9.1)	2.6 (1.3)	-	55.4
	86.1 (7.0)	2.1 (0.6)	89.7	
2-Loop	82.8 (11.2)	2.7 (1.7)	-	1.5
	85.9 (8.3)	2.1 (0.7)	88.8	

Table 2. Comparison with state-of-the-art approaches.

	Dice (%)	AV (mm)	% Good
Huang et al. [15]	89 (4)	2.2 (0.5)	79.2
Gopal et al. [16]	84 (4)	3.7 (0.6)	-
Ehrhardt et al. [17]	83 (NA)	1.8 (0.7)	-
Santiago et al. [18]	79 (8)	3.5 (1.4)	-
2-Loop	85.9 (8.3)	2.1 (0.7)	88.8

Table 2 shows a comparison between the proposed approach and some other related methods available in the literature. The segmentation assumptions in these methods are different from ours. [15] relies on an image based method, whilst [16, 17, 18] are based on a deformable models incorporating shape information. From Table 2, it is possible to see that the accuracy of the proposed method is competitive to all the other state-of-the-art approaches. Notice however that the proposed approach uses negligible shape information when compared with [16, 17, 18]. Also note that although in [15] achieves remarkable performance, the percentage of "good" results is considerable smaller then ours.

Fig. 3 summarizes the performance of the 2-Loop approach regarding the Dice coefficient. The image shown has 33×20 pixels, which correspond to the results for each of the 33 patients and each of the 20 volumes contained in each sequence. From the figure, the main conclusion is that the majority of the volumes are accurately segmented (see green color of each pixel of the image). Poorer segmentations are easily depicted in red. Also note that the algorithm exhibits better results in the diastole phase (see frames/columns 1-5 and 11-20) than in the systolic phase (frames/columns 6-10). This is somehow expected since the edges located at the LV border are brighter in these frames. The segmentation failures (depicted in red) are mainly due to the presence of papillary muscles. Fig. 4 shows examples of the segmentations obtained, in which it is possible to see many accurate segmentation, as well as poorer segmentations cause by the presence of papillary muscles (bottom right) or because the segmentation was pulled towards the LV's outer border (bottom left). These cases are hard to segment using an edge-based approach, since the strongest edges are not located on the LV border.
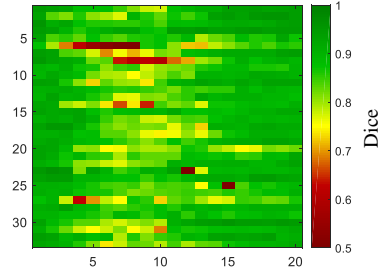

Fig. 3. Discriminative evaluation of the segmentation of each volume in the dataset (33 patients × 20 frames). The colormap indicates the Dice coefficient (greener is better).
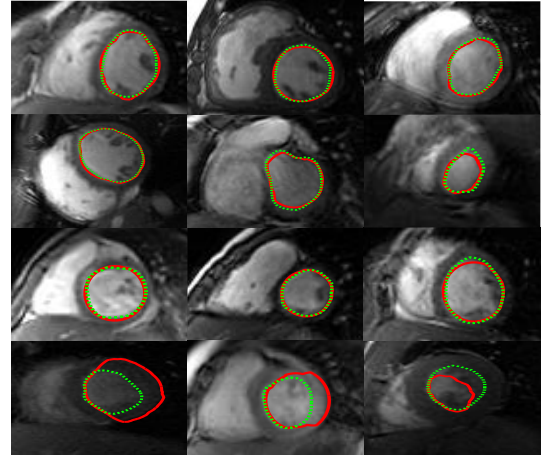

Fig. 4. Examples of segmentations obtained using 2-Loop (in red) and comparison with the GT (green). Each image shows one slice from a particular patient.

6. CONCLUSIONS

In this paper we proposed a fast and accurate approach for the segmentation of the LV in MR. The underlying idea of the approach is that the segmentation of each slice in the LV volume approximately has a circular shape. This fact suggests the use of the edge map in polar coordinates, whose valleys roughly correspond to the location of the LV boundary. The delineation of the LV contour is obtained using a dynamic programming algorithm. It is shown that the above strategy is able to achieve remarkable results concerning both accuracy and run time figures. Concerning the latter, the proposed method requires only 1.5 sec. to provide an accurate segmentation of the whole volume. This suggests that the proposed methodology can be a helpful tool to speed up the delineation of the LV contour in the clinical setup. Also, it is shown that the proposed approach is competitive with recent state-of-the-art approaches, which make more complex assumptions. Future work should focus on alternative ways to compute the edge map, in order to cope with the presence of papillary muscles more robustly.

7. REFERENCES

[1] J. M. B. Dias and J. M. N. Leitao, "Wall position and thickness estimation from sequences of echocardiographic images," *IEEE Transactions on Medical Imaging*, vol. 15, no. 1, pp. 25–38, Feb 1996.

[2] J. S. Marques and P. Pina, "Crater delineation by dynamic programming," *IEEE Geoscience and Remote Sensing Letters*, vol. 12, no. 7, pp. 1581–1585, 2015.

[3] C. Petitjean and J. Dacher, "A review of segmentation methods in short axis cardiac MR images," *Medical image analysis*, vol. 15, no. 2, pp. 169–184, 2011.

[4] V. Tavakoli and A. A. Amini, "A survey of shaped-based registration and segmentation techniques for cardiac images," *Computer Vision and Image Understanding*, vol. 117, no. 9, pp. 966–989, 2013.

[5] X. Lin, B. R. Cowan, and A. A. Young, "Automated detection of left ventricle in 4D MR images: experience from a large study," in *International Conference on Medical Image Computing and Computer-Assisted Intervention*. Springer, 2006, pp. 728–735.

[6] J. Cousty, L. Najman, M. Couprie, S. Clément-Guinaudeau, T. Goissen, and J. Garot, "Segmentation of 4D cardiac MRI: Automated method based on spatio-temporal watershed cuts," *Image and Vision Computing*, vol. 28, no. 8, pp. 1229–1243, 2010.

[7] A. Katouzian, A. Prakash, and E. Konofagou, "A new automated technique for left-and right-ventricular segmentation in magnetic resonance imaging," in *Engineering in Medicine and Biology Society, 2006. EMBS'06. 28th Annual International Conference of the IEEE*. IEEE, 2006, pp. 3074–3077.

[8] D. Geiger, A. Gupta, L. A. Costa, and J. Vlontzos, "Dynamic programming for detecting, tracking, and matching deformable contours," *IEEE Transactions on Pattern Analysis and Machine Intelligence*, vol. 17, no. 3, pp. 294–302, 1995.

[9] J. C. Fu, J. W. Chai, and S. T. C. Wong, "Wavelet-based enhancement for detection of left ventricular myocardial boundaries in magnetic resonance images," *Magnetic resonance imaging*, vol. 18, no. 9, pp. 1135–1141, 2000.

[10] J. Yeh, J. C. Fu, C. C. Wu, H. M. Lin, and J. W. Chai, "Myocardial border detection by branch-and-bound dynamic programming in magnetic resonance images," *Computer methods and programs in biomedicine*, vol. 79, no. 1, pp. 19–29, 2005.

[11] R. Szeliski, *Computer vision: algorithms and applications*, Springer Science & Business Media, 2010.

[12] A. Blake and M. Isard, *Active contours: the application of techniques from graphics, vision, control theory and statistics to visual tracking of shapes in motion*, Springer Science & Business Media, 2012.

[13] J. C. Nascimento and J. S. Marques, "Adaptive snakes using the EM algorithm," *IEEE Transactions on Image Processing*, vol. 14, no. 11, pp. 1678–1686, 2005.

[14] A. Andreopoulos and J. K. Tsotsos, "Efficient and generalizable statistical models of shape and appearance for analysis of cardiac MRI," *Medical Image Analysis*, vol. 12, no. 3, pp. 335–357, 2008.

[15] S. Huang, J. Liu, L. C. Lee, S. K. Venkatesh, L. L. San Teo, C. Au, and W. L. Nowinski, "An image-based comprehensive approach for automatic segmentation of left ventricle from cardiac short axis cine MR images," *Journal of digital imaging*, vol. 24, no. 4, pp. 598–608, 2011.

[16] S. Gopal and D. Terzopoulos, "A unified statistical/deterministic deformable model for LV segmentation in cardiac MRI," in *International Workshop on Statistical Atlases and Computational Models of the Heart*. Springer, 2013, pp. 180–187.

[17] J. Ehrhardt, T. Kepp, A. Schmidt-Richberg, and H. Handels, "Joint multi-object registration and segmentation of left and right cardiac ventricles in 4D cine MRI," in *SPIE Medical Imaging*. International Society for Optics and Photonics, 2014, pp. 90340M–90340M.

[18] C. Santiago, J. C. Nascimento, and J. S. Marques, "2D segmentation using a robust active shape model with the EM algorithm," *IEEE Transactions on Image Processing*, vol. 24, no. 8, pp. 2592–2601, 2015.